Science of the Total Environment 838 (2022) 156035

Contents lists available at ScienceDirect

Science of the Total Environment

journal homepage: www.elsevier.com/locate/scitotenv

Human footprints at hadal depths: interlayer and intralayer comparison of sediment cores from the Kuril Kamchatka trench

Serena M. Abel [a,b,c,*], Sebastian Primpke [b], Fangzhu Wu [b], Angelika Brandt [a,c], Gunnar Gerdts [b]

[a] Senckenberg Research Institute and Natural History Museum, Department of Marine Zoology, Senckenberganlage 25, 60325 Frankfurt am Main, Germany
[b] Department of Microbial Ecology, Biologische Anstalt Helgoland, Alfred Wegener Institute, Helmholtz Centre for Polar and Marine Research, Kurpromenade 201, 27498 Helgoland, Germany
[c] Goethe University Frankfurt, Institute for Ecology, Diversity and Evolution, Max-von-Laue-Straße 13, 60438 Frankfurt am Main, Germany

HIGHLIGHTS

- Thirteen sediment cores were collected from the KKT between 5740 and 9450 m depth.
- Overall, 215 to 1596 MP kg $^{-1}$ were detected, 72% of these were smaller than 25 μm.
- Fourteen polymer types were detected, mainly acrylates/PUR/varnish, PP, PE and PA.
- Intralayer and interlayer core comparisons highlighted a heterogeneous MP distribution.
- The adapted MP processing procedure permitted a higher detection of small MP.

GRAPHICAL ABSTRACT

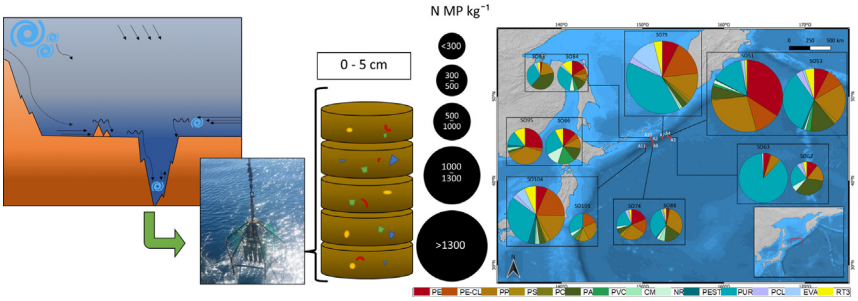

ARTICLE INFO

Editor: Rafael Mateo Soria

Keywords:
Microplastic pollution
Spectroscopic analysis
Density separation
Deep sea sediments
Hadal trenches
Sedimentation dynamics

ABSTRACT

Microplastic (MP) pollution affects almost all ecosystems on Earth. Given the increasing plastic production worldwide and the durability of these polymers, concerns arise about the fate of this material in the environment. A candidate to consider as a depositional final sink of MP is the sea floor and its deepest representatives, hadal trenches, as ultimate sinks. In this study, 13 sediment samples were collected with a multiple-corer at depths between 5740 and 9450 m from the Kuril Kamchatka trench (KKT), in the Northwest (NW) Pacific Ocean. These samples were analysed for MP presence in the upper sediment layer, by slicing the first 5 cm of sediment cores into 1 cm horizontal layers. These were compared against each other and between the sampling areas, in order to achieve a detailed picture of the depositional system of the trench and small-scale perturbations such as bioturbation. The analyses revealed the presence of 215 to 1596 MP particles per kg $^{-1}$ sediment (dry weight), with a polymer composition represented by 14 polymer types and the prevalence of particles smaller than 25 μm. A heterogeneous microplastic distribution through the sediment column and different microplastic concentration and polymer types among sampling stations located in different areas of the trench reflects the dynamics of this environment and the numerous forces that drive the deposition processes and the in situ recast of this pollutant at the trench floor.

1. Introduction

Microplastic (MP) pollution, is demonstrated to affect the majority of the marine realm, at all latitudes, longitudes and depths (Bucol et al., 2020; Kelly et al., 2020; La Daana et al., 2020; Peeken et al., 2018; Reed et al., 2018; Roscher et al., 2021a). The ubiquity and the long-lasting durability of plastics, together with the global increase of its production

* Corresponding author at: Department of Microbial Ecology, Biologische Anstalt Helgoland, Alfred Wegener Institute, Helmholtz Centre for Polar and Marine Research, Kurpromenade 201, 27498 Helgoland, Germany.
E-mail address: serena.abel@awi.de (S.M. Abel).

http://dx.doi.org/10.1016/j.scitotenv.2022.156035
Received 17 February 2022; Received in revised form 11 May 2022; Accepted 14 May 2022
Available online 20 May 2022

(Nakajima et al., 2021; Dai et al., 2018), are major causes for concern in the scientific community.

It is estimated that 2.4 to 4.0 million tons plastic enter the marine environment though the rivers yearly (Lebreton et al., 2017; Schmidt et al., 2017), from this a considerable portion sinks to the seafloor (Cózar et al., 2014), accumulates in marine sediment (Andrady, 2011; Kane et al., 2020), or is transported by bottom currents and ocean internal hydrodynamic events until it reaches its ultimate destination: the hadal sea floor.

The ubiquity of marine MP pollution is the consequence of atmospheric, oceanographic and biological processes causing the transport and dispersion of MP at each water depth (Petersen and Hubbart, 2021; Matsushita et al., 2021). Wind driven surface currents and the main oceanic water currents are responsible for a long-distance transport, from land-born sources to the open ocean (Obbard, 2018; Ryan, 2020). Vectors causing vertical mixing such as waves, turbulences like gyres and eddies, downwelling phenomena and thermohaline circulation, drive the transport of MP through the water column to the seafloor (Kane and Clare, 2019a; Cincinelli et al., 2019). Even in this environment the final destination of MP is not settled, as bottom currents, turbidites, and seismic events can cause the dispersion, burying and resuspension of MP particles (Pohl et al., 2020; Peng et al., 2018b).

Biota and biological processes, such as biofouling and the inclusion of MP in organic aggregates and colloid substances (fecal pellets, marine snow, phytodetritus, exopolymer particles) also contribute to modifications in MP transport pathways by increasing the sinking rates of MP, including those of low-density polymers (Zhao et al., 2017; Kvale et al., 2020a; Porter et al., 2018). On the seafloor, the actions of meio- and macrobenthos lead to the dispersion of MP and their inclusion in the deeper sediment layers by bioturbation (Courtene-Jones et al., 2017; Näkki et al., 2017). It is documented that in geographic areas with high anthropogenic activities, the anthropogenic footprint is more persistent and MP accumulation in sediments might reach considerably high levels (Dai et al., 2018). The Northwest Pacific Ocean is one of the major transit pathways for marine litter that is entering the North Pacific Ocean from Asia (Nakajima et al., 2021). Moreover, the Kuril Islands and their straits are intensely utilized for fishing and shipping activities (Klovach et al., 2021). Therefore, it's deepest point, the Kuril Kamchatka trench (KKT), would likely accumulate sinking MP and marine litter and be the final sink and a potential hotspot of MP (Peng et al., 2020). Specific hydrodynamic conditions and geological activities favor MP accumulation in the trench, both consequent to the vicinity of the KKT to the Kuril Islands. This island arc is considered as a water body transition area, in which transport and mixing processes between the Sea of Okhotsk and the North Pacific, via the Kuril straits, are taking place. In this area, massive turbulences and vorticity occur in the water column, all the way down to the seafloor (Yagi and Yasuda, 2012, 2013), causing considerable sediment resuspension and recasting in the areas adjacent to the island arc. The Kuril Kamchatka arc system is also described as the most mobile and seismically active region in Northeast Eurasia. The underlying sea floor is the showplace of modern tectonic and volcanic processes, including earthquake driven sub marine fan turbidities (Aksentov and Sattarova, 2020; Avdeiko et al., 2007; Braitseva et al., 1995; CORMIER, 1975; Fischer and Yang, 1994; Steblov et al., 2010). Additionally, deep flows on the slope inshore of the trench were observed in oceanographic studies (Uehara and Miyake, 1999) and combined, together with the above listed geological and hydrological processes, drive the resuspension of sediment and particulate material, including MP, in the trench system. One of the principal Northwest Pacific currents, the northwards Kuroshio current, reaches the Kuril region, transporting with its nutrients (Saito, 2019) as well as anthropogenic litter (Nishizawa et al., 2021; Shiu et al., 2021; Nakajima et al., 2021). On one hand, the current provides a constant nutrient supply for benthic communities in this region, which are reliant on sinking nutrients form the water column (Golovan et al., 2019). On the other hand, it is a consistent long-distance transport path by which MP (Kalak, 2018) reach the geographic region of the trench.

Preliminary studies highlighted the presence of anthropogenic litter in the KKT and the identification of MP was performed in the abyssal and hadal sediments of the trench (Abel et al., 2021) confirming the presence of MP in the deepest part of the trench. Several deep-sea related studies further identified MP in other Pacific trenches (Jamieson et al., 2019b; Zhang et al., 2020), hypothesizing that this environment could indeed act as an ultimate sink for MP pollution.

On this background, our study aims to (1) provide the baseline for the understanding of MP sedimentation in deep sea trenches, (2) foster a better understanding of the unique dynamics in this remote area and (3) highlight the importance of a tailored MP extraction method by comparing analyses based on the same physical and chemical principles.

2. Material and methods

2.1. Sediment sampling

Thirteen sediment cores were collected from the KKT from seven sampling areas (A2, A3, A4, A9, A10, A11, A7) in summer 2016, on-board the RV *Sonne* during a deep-sea expedition (SO-250 Kurambio II). Every area, except A7, was sampled twice, by using a Multiple-Corer (MUC 2011–124 K2 x100; OKTOPUS GmbH, Kiel, Germany; 12 core tubes, inner Ø: 95 mm, length: 600 mm, material: stainless steel, PC), and is therefore represented by two sediment cores each. A7 is represented by one core due to complications during the sampling event. Further details of the sampling areas are provided in Fig. 1.

Onboard, the first 5 cm of each sediment core were sliced into 1 cm layers and stored separately in PVC bottles (Kautex Textron GmbH and Co KG, Bonn, Germany), and immediately frozen at −20 °C. Furthermore, the water layer above the sediment present in the MUC, a volume ranging between 50 and 710 mL, was collected and stored in the same way.

2.2. Sample preparation and processing

Prior to MP identification, several preparatory steps were required, based on density separation and organic material digestion. The five sediment horizons representing each core, the water layer above the sediment, as well as a procedural blank, were all processed simultaneously.

Each sediment layer was defrosted, and transferred to a pre-weighed beaker (weights of the samples are listed in SI). The samples were then dried for four days at 60 °C, covered with aluminium foil. The dry samples were weighted and the backers weight subtracted to determine the dry weight (DW) of the sample. Subsequently, the samples were sieved with a 500 μm stainless steel mesh. Both fractions, larger and smaller than 500 μm were weighed, then the >500 μm fractions were transferred to glass Petri dishes and stored for further analysis.

2.2.1. Processing of the <500 μm fraction

2.2.1.1. First density separation. The density-based separation step in this study was inspired by two MP extraction methods: the density separation via MPSS (MicroPlastic Sediment Separator, Hydro-Bios), (Imhof et al., 2012b) and the principle of overflow to collect lighter sample fraction applied by Mani et al. (2019). For the initial density separation, the sample material was mixed with a sodium bromide (NaBr) solution (density 1.6 g cm^{-3}) (Quinn et al., 2017) (99.5% purity, Grüssing GmbH, Diagnostica Analytika, Flisum, Germany) and transferred into glass culture-media bottles with straight neck (300 mL Duran), filled to 2.5 cm below the brim, and covered with an aluminium cup.

To disaggregate sediment agglomerates, the bottles were submerged in an ultrasonic bath, with the brim of the bottle 3 cm from the water surface, and sonicated for 15 min at 160 W/35 KHz (Sonorex RK255 H, Bandelin Electronic GmbH & Co., Berlin, Germany).

The samples were then stirred with a magnetic stirrer (C-MAG HS control, IKA, Germany, stir bar: Bola Beakerliner, PTFE, Omnilab-Laborzentrum GmbH & Co. KG; Germany) for 1 h at 350–450 rpm. Before placing the bottles in the laminar flow cabinet (ScanLaf Fortuna, 1800;

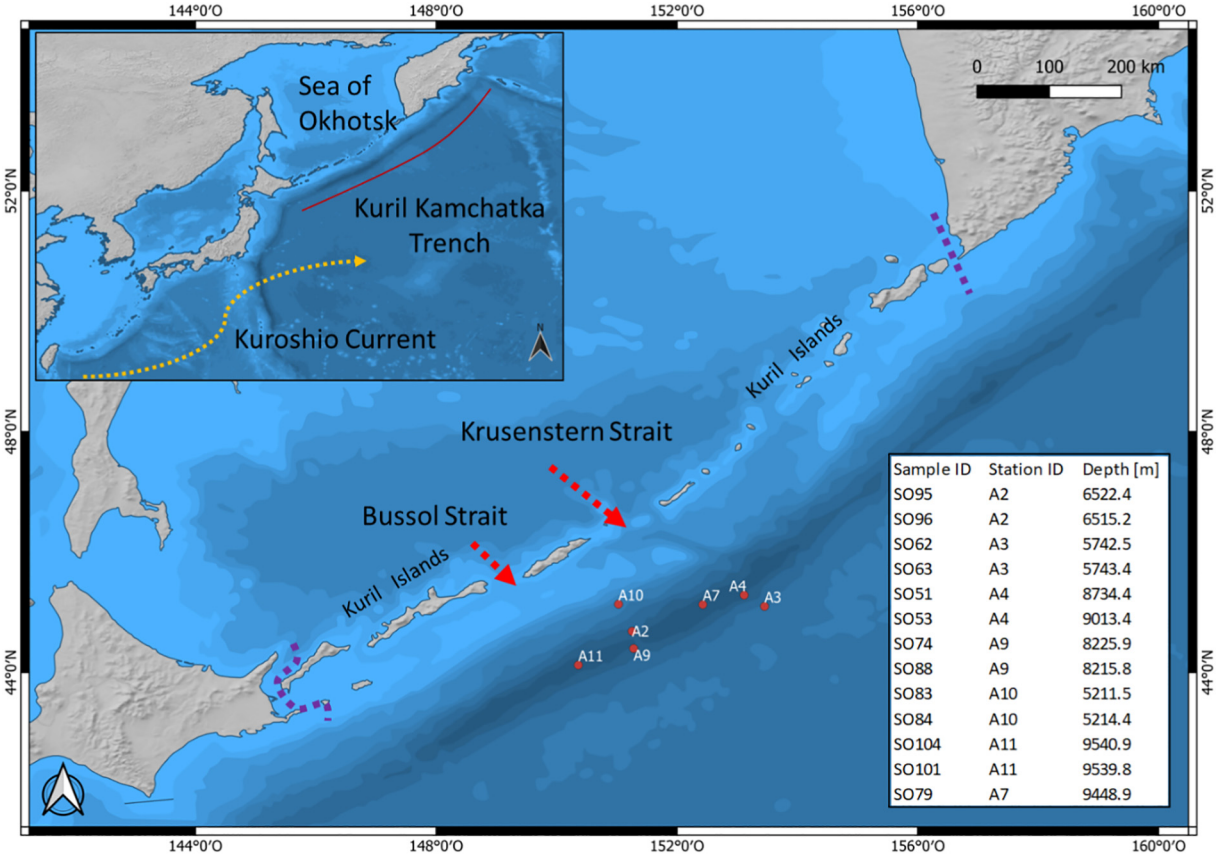

Fig. 1. List of samples (Sample ID), sampling areas (Station ID) and sampling depth in meters. Red dots on the map depict the location of the sampling area in the trench, the red line underlines the trench extension, yellow dashed arrow represents the Kuroshio Current, red dashed arrows underline the Krusentern and Bussol straits, purple dashed lines indicate the limit of the Kuril Island arc system.

LaboGene, Lillerød, Denmark), the external walls of the bottles were cleaned using an airbrush (Airbrushgun Typ 180, WilTec Wildanger Technik GmbH, Germany), to remove potential airborne contamination. The bottles were then placed into PTFE evaporating basins with flat bottoms (height 36 mm, Ø ext. 132 mm, VWR International GmbH, Germany) and the sample was left settle to allow the density separation process, until the liquid column clear. The settling time depended on the sedimentation time of the denser fraction and ranged between 60 and 120 min.

To separate the lighter material from the denser sediment, 90 mL NaBr solution was added to each sample at around half the height of the liquid column by using glass syringes (50 mL, Carl Roth GmbH + Co. KG, Germany). Adding the NaBr solution at this level, leads to the overflow of the lighter particles, which were then collected in the evaporating basins, without causing the resuspension of the settled heavier material. After the overflow, the solution in the bottle was partially removed to prevent it from ending in the evaporation basins. The syringe needle, the external walls and the bottom of the bottles were then rinsed carefully with 0.22 μm filtered Milli-Q ultrapure water (Milli-Q water) and the rinsing water was collected in the evaporating basins.

The collected particles were filtered onto stainless-steel meshes (pore size 20 μm, Ø 47 mm, HAVER & BOECKER OHG) and flushed with Milli-Q water to remove residues of the NaBr solution. The main steps of the procedure are illustrated in SI.

2.2.1.2. Fenton treatment and second density separation. Fenton reaction was carried out following the protocol suggested in studies by Tagg et al. (2017), Bergmann et al. (2017a), Hurley et al. (2018), Tekman et al. (2020) and Abel et al. (2021), and are descried in detail in SI. After the Fenton reaction, the treated samples were removed from the filters by placing them in 150 mL glass beakers containing 50 mL of NaBr solution and sonicated for 5 min at 160 W / 35KHz. The filters and the beakers were rinsed with NaBr solution to collect the adhered particles and the suspended treated samples underwent a second density separation to remove any remaining inorganic material. For this, the NaBr- sample suspensions were transferred into glass separation funnels (50 mL LabMarket GmbH, Germany) and placed within a laminar flow cabinet. After 12 h, the lower fraction in the funnel was discarded. New NaBr added, to reach the initial volume of 50 mL, and to resuspend eventual particles stick to the glass walls. This procedure was repeated twice, after a further 4 h and 8 h settling time. After this time, the remaining sample solutions were filtered onto stainless-steel filters (pore size 20 μm, diameter 47 mm), and flushed with Milli-Q water to remove any NaBr residues from the samples. Finally, the sample material from the filters was resuspended in Milli-Q water and these processed samples were stored in 250 mL wide neck glass bottles (Duran) until analysis.

2.2.1.3. Analytical filter preparation for <500 μm fraction. To establish the particle concentration in the treated sample suspensions, a FlowCam (Fluid Imaging Technologies, Portable version IV, Scarborough, Maine, US) was used to quantify the particle concentration in a subsample (100 μL) (Abel et al., 2021; Lorenz et al., 2016; Bergmann et al., 2019). This concentration values were then applied to calculate the sample volumes that would be suitable for individual FTIR measurement. Ideally, this optimal sample volume results in a full coverage of the aluminium-oxide filters (Anodisc, 0.2 μm pore size, 25 mm diameter Whatman) used for FPA-μFTIR analyses (Lorenz et al., 2017; Primpke et al., 2020; Tekman et al., 2017). Subsequently, each of the samples was vacuum filtered, in its entirety, onto the determined number of aluminium-oxide filters and placed in a desiccator cabinet (Bohlender Star-Vitrum, V1841–07) overnight prior to FTIR measurement.

2.2.1.4. MP identification of small microplastics (S-MP, <500 μm). In accordance to Primpke et al. (2017) an FPA (Focal Plane Array) -based micro Fourier Transform Infrared (μFTIR) hyperspectral-imaging approach was applied for the chemical identification, quantification and sizing of S-MP. The μFTIR measurement was performed using a Bruker TENSOR II spectrometer, with a 64 × 64 FPA detector Hyperion 3000 μFTIR-microscope (Bruker Optics GmbH, Ettlingen, Germany). Before the measurement, Anodisc filters were covered with a BaF_2 window, compressing all items into the narrow focal plane of the FTIR microscope, which especially enhances the assessment of fibre-like MP (Primpke et al., 2019). The FTIR measurements were performed using 3.5 x objective (Bruker Optics GmbH, Ettlingen, Germany) at a spectral resolution of 8 cm^{-1} and 32 co-added scans, Blackman-Harris 3-term apodization, zero filling factor of two and Power/ No peak search for phase correction. With this setup, a pixel size of 11.69 × 11.69 μm per spectra was achieved and an area of 22 × 22 FPA fields measured. All data were collected using Bruker software OPUS 8.5 (Bruker Optics GmbH, Germany).

SiMPle database (version 1.0. β) (Primpke et al., 2020) was applied for the polymer identification for the automated analysis of all datasets (Primpke et al., 2020). Pixels assigned to the Polypropylene (PP) edge of the Anodisc filter were removed using the circular mask function within the heatmap feature application within siMPle (Primpke et al., 2019). Finally, in order to obtain the final data on S-MP numbers, sizes and assigned polymer cluster, an image analysis in MPAPP (version 1.1.1) was performed.

2.2.2. Sorting and analysis of large microplastics (L-MP, 500–5000 μm)

Putative L-MP were manually sorted out from the >500 μm sample fraction by using a stereomicroscope at 100-400× magnification. All putative L-MP (fibres and particles) were transferred into glass petri dishes, photographed and measured (length at their longest dimension and the orthogonal dimension at their widest point) under the stereo microscope (Olympus DP26 Digital Camera, Olympus) using image analysis software (CellSens, Olympus). Subsequently, all particles and fibres were identified individually using an Attenuated Total Reflection (ATR) FTIR spectrometer (Bruker Tensor 27 coupled to diamond platinum ATR unit, Bruker Optik GmbH, Germany) (Roscher et al., 2021b; Lorenz et al., 2021), with a Blackman-Harris 3-term apodization and zero filling factor of two. The IR spectra were collected in the spectral range of 400–4000 cm^{-1} and compared against a reference library (Primpke et al., 2018). Particles with a match of at least 700 (out of 1000) were counted as effectively identified. Particles with a lower match (between 600 and 700) were manually compared to database spectra and manually re-evaluated leading to confirmation or rejection (Roscher et al., 2021b). Particles with a match below 600 were rejected and considered as undefinable.

2.3. Quality assurance and quality control

Contamination prevention was considered during the whole analysis pipeline. While handling and processing the samples 100% cotton laboratory coats were worn to reduce possible contamination with fibres from clothing, additionally, fibre samples from all the clothes worn during the laboratory analysis steps were collected and analysed by ATR- FTIR spectrometer (Bruker Tensor 27 coupled to diamond platinum ATR unit, Bruker Optik GmbH, Germany) to exclude them as potential fibre contamination sources. Hands were carefully washed before every procedural step and no nitrile gloves were worn during the entire analysis pipeline (Witzig et al., 2020). All reagents (e.g., $FeSO_4$ solution, H_2O_2, HCl and NaBr solution) were filtered through glass microfiber filters (0.2 μm pore size, Ø 47 mm, Whatman, Germany) and all equipment used were made of glass or stainless steel. Equipment and surfaces were carefully rinsed with Milli-Q water and cleaned with an airbrush prior to use. To minimize airborne contamination all the preparatory steps were carried out in a laminar flow cabinet (ScanLaf Fortuna, 1800; LaboGene, Lillerød, Denmark). The only exception was the initial stirring step, performed on the laboratory bench. Here, contamination was avoided by closing the glass culture-media bottles with aluminium lids before moving them out of the flow cabinet. Dust box air-filters (DB1000, G4 prefiltration, HEPA-H14 final filtration, Q ¼ 950 m^3 h^{-1}, Mocklinghoff Lufttechnik, Gelsenkirchen, Germany) were active in all laboratories. Finally, blank samples analyses were conducted and confirmed that no contamination from the use of plastic storage bottles has occurred.

2.4. Statistical analysis

MP concentrations and polymer types were considered for statistical analysis: Pearson correlation was calculated to verify any correlation between these variables with; 1) sediment composition, including sediment granulometry (clay, silt and sand) and total organic carbon (TOC); 2) distribution in the sediment column; and 3) sampling stations at different depths. Pearson correlation was calculated to verify any correlation between sediment granulometry and TOC with the sediment depth and station depth. Sediment composition related data (TOC and sediment granulometry) originated from geochemical and physical analyses carried out by the V.I. Il'ichev Pacific Oceanological Institute team (Far Eastern Branch of Russian Academy of Sciences, Vladivostok 690,041, Russia) (Sattarova and Aksentov, 2021). The cores for geochemical and physical analysis were collected with the same MUC sampling as the cores used for MP analysis in this study, and provided information about granulometry and TOC of the first five cm of the sediment column of the following samples: SO62, SO51, SO74, SO101 and SO79 (Fig. 1).

Finally, one way ANOVA on ranks, based on a Kruskal-Wallis test, was applied to test whether the samples originate from the same distribution (Kane et al., 2020). To find out which layers were significantly different, a Dunn-Bonferroni Post Hoc test was run. All the statistical analyses were carried out via R (R development Core Team, version 4.1.2) and STATISTICA (StatSoft).

3. Results

3.1. Small microplastics (S-MP)

This study investigates MP in 13 sediment samples collected in the KKT between 5211 and 9541 m (Fig. 1). The samples weight ranged between 90 and 207 g (DW) Overall, between 215 and 1595 S-MP kg^{-1} were detected. In all cores, S-MP were predominantly particle-like shaped with a relative percentage ranging between 71 and 97%, while 3 to 29% were fibre-like MP. In total 14 different polymer types were identified, with acrylates/polyurethane/varnish (acrylates/PUR/varnish) and polypropylene (PP) as the most common polymer types, accounting for 34% and 19% of the total measured S-MP composition, respectively, followed by polyethylene (PE; 14%) polyamide (PA; 8%) and polyethylene chlorinated (PE-CL; 9%). Rubber type 3 (RT3), ethylene vinyl acetate (EVA), nitrile rubber (NR), polyvinylchloride (PVC), polycaprolactone (PCL) and polystyrene (PS) accounted, for 2.5% each, while polycarbonate (PC), chemically modified cellulose (CM) and polyester/polyethylene terephthalate (PEST) accounted each for less than 1% to the total measured S-MP composition (Fig. 2a).

On average, 45% of all detected S-MP were smaller than 11 μm, 27% ranged between 11 and 25 μm in size, 15% between 25 and 50 μm and 7% between 50 and 75 μm. The remaining 7% were larger than 75 μm, of these 2% were between 75 and 100 μm, and the remaining 5% were above 100 μm. No MP larger than 750 μm were identified. Considering the size of just the particle-like S-MP, no particles larger than 425 μm were detected, with all the MP larger than 425 μm being fibre-like in shape (Fig. 2b) S-MP concentration (MP kg^{-1}), number of polymers per sample (N pol) and polymer types (expressed in relative percentage, %) specified for every sample are listed in Table 1 and are represented graphically in Fig. 4a (red square).

S-MP distribution and polymer composition in sediment layers are displayed in Fig. 3, and listed in detail in SI.

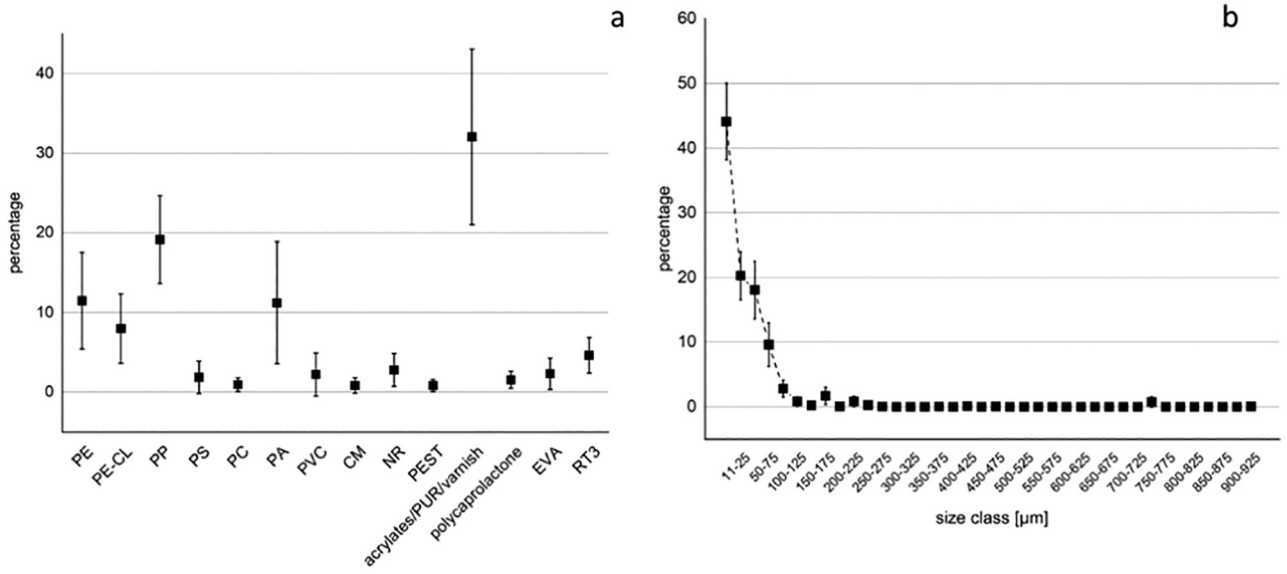

Fig. 2. (a) Mean percentage of each polymer type in all sediment samples (black square) PE: polyethylene, PE-CL: polyethylene chlorinated, PP: polypropylene, PS: polystyrene, PC: polycarbonate, PA: polyamide, PVC: polyvinyl chloride, CM: chemically modified cellulose, NR: nitrile rubber, PEST: polyester/polyethylene terephthalate, PUR: polyurethane, EVA: ethylene vinyl acetate, RT3: rubber type three. Error bars show the 95% confidence interval. (b) Mean percentage of each S-MP size class in µm from all sediment samples (squares). Error bars show the 95% confidence interval.

3.2. Large microplastics (L-MP)

In total nine particle-like and 35 fibre-like MP were categorised as putative L-MP, however, the spectral analysis revealed that just one transparent particle was identified as being a synthetic polymer, confirmed as PVC, with the dimensions 1758.7 µm × 421.5 µm. All the remaining particle-like and fibre-like putative L-MP were characterised as being not synthetic (mostly chitin coal, and plant fibres and animal fur).

3.3. Statistic results

Pearson correlations revealed negative correlations between silt and the station depth ($r = -0.484$; $p = 0.041$), and between TOC and station depth ($r = -0.592$; $p = 0.002$) in all the stations with granulometry and TOC data availability. The negative correlation was especially visible in A7 and A9 (Fig. 1) where the *r*-values were − 0.951 and − 0.990 and *p*-values 0.031 and 0.043 respectively. For the remining granulometric classes no correlations were established (Tables in SI).

Concerning MP composition and concentration, PE ($r = 0.671$; $p = 0.003$), PE-CL ($r = 0.440$; $p = 0.05$), PP ($r = 0.0515$; $p = 0.032$) correlate positively with the sediment class 'clay', whilst NR ($r = -0.4886$; $p = 0.001$) correlates negatively. PCL showed a positive correlation with the 'silt' class ($r = 0.489$; $p = 0.02$), and PVC showed a positive correlation with TOC ($r = 0.463$; $p = 0.04$).

Concerning the abundance of specific polymers through the sediment column, (0–5 cm), significant negative correlations with the sediment depth were detected overall for PS ($r = -0.254$; $p = 0.042$), PA ($r = -0.266$; $p =$ 0,032), PCL ($r = -0.314$; $p =$ 0,01) and RT3 ($r = -0.298$; $p =$ 0,005 TOC). Clear negative correlation trends were observed in A7 (core SO79) for PP ($r = -0.87$; $p = 0.048$) and in A11 (core SO104) for RT3 ($r = -0.979$; $p = 0.05$), while in A4 (core SO53) the correlation was positive for EVA ($r = 0.890$; $p = 0.038$). In all the cores, MP concentration had a slightly negative correlation with the sediment depth ($r = -0.298$ $p = 0.025$) and was clearly negative in SO62 ($r = -0.888$; $p = 0.012$). Finally, the polymer composition in SO79 showed a negative correlation with the sediment depth ($r = -0.991$ $p = 0.039$). One-way ANOVA on ranks, based on a Kruskal-Wallis test, revealed statistically significant differences in PCL distribution and in MP concentration through the sediment column. The post-hoc Dunn's test confirmed that PCL content in the first layer (the 0–1 cm of sediment) differed significantly from the second

Table 1
S-MP concentration (MP kg^{-1}), polymer diversity (N Pol) and relative percentage of polymer types detected in the analysed KKT sediment samples. PE: polyethylene, PE-CL: polyethylene chlorinated, PP: polypropylene, PS: polystyrene, PC: polycarbonate, PA: polyamide, PVC: polyvinyl chloride, CM: chemically modified cellulose, NR: nitrile rubber, PEST: polyester/polyethylene terephthalate, PUR: polyurethane, PCL: polycaprolactone, EVA: ethylene vinyl acetate, RT3: rubber type three.

Sample ID	Station ID	MP Kg-1	N pol	PE	PE-CL	PP	PS	PC	PA	PVC	CM	NR	PEST	PUR	PCL	EVA	RT3
SO95	A2	463	10	26%	3%	36%	2%	2%	1%		3%		2%	13%			10%
SO96	A2	464	8	12%	5%	10%			12%	16%		12%		25%			8%
SO62	A3	399	8	11%		16%			34%			6%		23%	5%	2%	4%
SO63	A3	892	6	5%	1%	6%	1%							1%		1%	
SO51	A4	1595	9	34%	11%	27%			6%	1%		2%		14%		2%	1%
SO53	A4	1321	13	8%	9%	20%	1%	1%	13%	3%		1%	1%	34%	4%	1%	5%
SO74	A9	315	9	19%	15%	26%	4%		6%			3%		19%	5%		3%
SO88	A9	383	11	3%	1%	31%			17%		5%	3%	1%	33%	2%	1%	3%
SO83	A10	215	6	2%		19%			40%					30%		3%	5%
SO84	A10	293	10	16%	6%	7%		2%	11%	5%		5%		33%		3%	12%
SO101	A11	230	7		17%	21%	11%	4%		4%		4%		28%			
SO104	A11	1150	13	7%	19%	16%	2%	1%	3%		2%	1%	4%	31%	2%	6%	7%
SO79	A7	1310	12	7%	16%	12%	1%	2%	2%		1%	1%		40%	3%	12%	4%

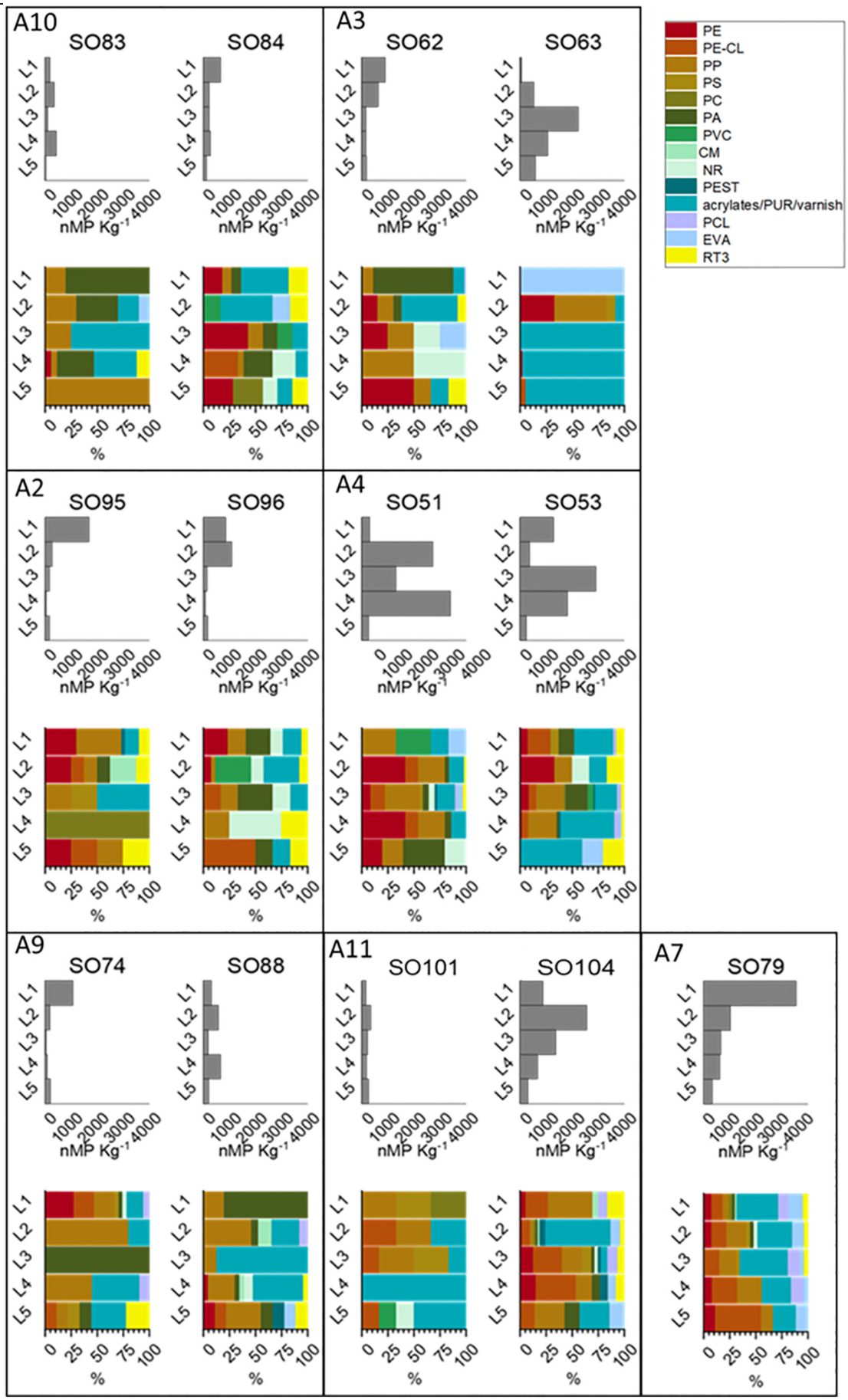
A10
SO83
SO84
A3
SO62
SO63
A2
SO95
SO96
A4
SO51
SO53
A9
SO74
SO88
A11
SO101
SO104
A7
SO79
L1
L2
L3
L4
L5
0
1000
2000
3000
4000
nMP Kg-1
0
25
50
75
100
%
PE
PE-CL
PP
PS
PC
PA
PVC
CM
NR
PEST
acrylates/PUR/varnish
PCL
EVA
RT3

layer (1–2 cm) and the fifth layer (4–5 cm), while the post- hoc analysis on MP concentration distribution in the layers didn't reveal any significant differences (see SI for more details).

4. Discussion

4.1. Interstudy comparison

Given the variety of environmental samples and MP processing methods, comparing the results of different studies is still one of the main criticisms in this research field (Cashman et al., 2020). Nevertheless, comparisons between analyses based on the same physical and chemical principles can consistently help improve the methods of MP analysis by supplementing potentially critical or bias-prone steps. In this context, it is essential to underline the importance of the choice of suitable MP processing methods, based on the characteristics of a sample. Inferences were drawn by comparing our outcomes with those of an earlier study on MP identification in abyssal and hadal sediments of the KKT (Abel et al., 2021) utilising a comparable, density separation-based, approach. Abel et al. (2021) aimed to determine and characterize MP contamination in the first 5 cm of sediment column from four sampling areas, represented by a total of eight samples, using a Munich Plastic Sediment Separator (MPSS). The MP concentration from this study ranged from between 14 and 209 MP kg^{-1} (DW), with 15 polymer types identified overall, and a polymer diversity per sample ranging between four and seven (Fig. 4a, in yellow). By comparing these values with the ones achieved in our present study, the MP concentration and polymer diversity in the samples were decidedly different, being higher in the current study, with concentrations ranging from 215 to 1596 MP kg^{-1} (DW) and a sample polymer diversity of between six and 13 (Fig. 4a, in red). The total polymer diversity, however, differed by only one polymer type (15 in Abel et al. (2021), 14 in this study), suggesting that the different polymers are not specifically affected by one technique rather than the other, but that the MP concentration data are (Fig. 4b). See SI for further comparison of the differences in MP concentration and polymer diversity between the two studies. These discrepancies in the concentration data result from a higher recovery efficiency of the method applied in our current study rather than a higher MP concentration in the sample.

4.2. Processing procedure comparison

As deductible from the comparison of the MP size-class distribution in the two studies, the MP size target of a processing method has a high influence on the outcomes of MP detection in environmental-matrices studies. Despite that in both studies MP belonging to the lowest size range (<11 μm) are the most represented, the relative percentage of particles in the lowest size range of the present study is around 10% higher than that of the earlier study (Abel et al., 2021) (Fig. 4c). This discrepancy between the size distributions could be attributed to MP particle loss during the purification step when using the MPSS, especially for those MP representing the lower size class.

The MPSS remains one of the most suitable devices for MP processing for large quantities of sediment (1–6 kg) (Imhof et al., 2012a), as demonstrated by the numerous previous studies that used this device or that took inspiration from its design. (Bergmann et al., 2017a; Bergmann et al., 2017b; Coppock et al., 2017; Haave et al., 2019; Lorenz, 2014; Mahat, 2017; Stock et al., 2019).

A recent study tested the MP processing efficiency of the MPSS, with the lowest size limit set at 40 μm, achieving a recovery rate efficiency of 95.5% for MP smaller than 1 mm (Imhof et al., 2012a). The size class distribution from a previous study (Abel et al., 2021), highlighted that 71.1% of all detected MP were <25 μm in size, therefore would not have been included in the processing evaluation by Imhof et al. (2012a). Furthermore, in the evaluation experiment, natural sediment, cleaned of MP contamination using sequential $ZnCl_2$ processing and deionised water rinses, was subsequently enriched with primary and secondary MP. The recovery of these environmentally relevant plastic types from the treated sediment was used to test the efficiency of the MPSS. As highlighted by another study (Zobkov et al., 2017), the MP recovery rate via MPSS can be reduced by 50% when using natural, rather than treated, marine sediment. Moreover, high volumes of sediment, combined with an inefficient agitation time, reduces the processing efficiency (Filgueiras et al., 2021). This is caused, among other factors, by a screening effect of the dense mineral component of the sediment at the bottom of the MPSS on underlying lighter material, that is therefore, prevented from resuspension and separation. Furthermore, agglomerates of material can include MP polymers and prevent them from reaching the upper collecting chamber, instead of remaining suspended at a lower level of the density separation column. Even when sampling the suspended material from the collecting chamber, further particle loss could occur, as there is the risk that small particles become entrapped in the ball valve fitting. There is also the possibility of the $ZnCl_2$ solution reacting with carbonate compounds and shelf fragments present in the sediment, producing gases such as CO_2, and leading to foam formation. Separated MP particles can become trapped in this foam and are easily lost if excessive foaming overspills the collection chamber.

In the present study, based on the methodology of Mani et al. (2019) for MP processing from sediments, we attempted to avoid the above described weaknesses in the MPSS technique. By analysing small amounts of sediment, given the intrinsic necessity to study the individual sediment layers of the cores, many of the issues of bulk sediment processing were further negated. To avoid the negative effects of particle agglomeration, an ultrasonification step was applied, prior to the density separation, to disaggregate the sediment. During the mixing step of the density separation, the speed of the magnetic stirrers was set in such a way as to cause all the sediment to become suspended. As the required speed to achieve a complete suspension of the material was strongly dependent on the grain size of the sample, this was easily adjusted by observing the degree of suspension in the glass bottles and optimising it for every sample. Using a glass bottle for the initial density separation steps also had the advantage of being a simple receptacle with straight walls, thus avoiding the aforementioned risks associated with particle loss in the multiple components and connections of the MPSS. The optimisation of the processing method in this study led to a higher recovery of small MP than when using the MPSS, confirmed by a higher relative percentage of MP in the present study.

4.3. Use of NaBr for density separation

In this study, a NaBr solution (density 1.6 g cm^{-1}) was chosen as the separation solution for the MP extraction step. The different fluidic and chemical proprieties of the brine solutions used for MP density separation, NaBr and $ZnCl_2$ in this case, can also concur to explain the higher number of MP extracted in this study, compared to that of Abel et al. (2021). The evaluation of MP presence in the trench from the previous study, highlighted the presence of a considerable percentage of small MP (99% smaller than 125 μm). $ZnCl_2$ has a higher recovery rate for the upper MP size class range, whereas NaBr has a recovery rate described as inversely proportional to MP size (Quinn et al., 2017), and is relatively high, regardless of the shape and size of the particles (Liu et al., 2019). From the point of view of the user, NaBr has a lower toxicity than $ZnCl_2$ and is less viscous and sticky, making its use generally more practical and preferable.

Fig. 3. Panels displaying the S-MP concentration (in MP kg^{-1} sediment, dry weight) and the polymer composition (in relative percentage) of the five, 1 cm thick, sediment layers (L1 to L5) of the 13 sediment cores analysed. In every panel are displayed the results from two cores collected from the same area: A10, A3, A2, A4, A9, A11, A7. The order of arrangement the panels in the figure is related to the sampling depth, from shallow to deep. PE: polyethylene, PP: polypropylene, PS: polystyrene, PC: polycarbonate, PA: polyamide, PVC: polyvinyl chloride, PEST: polyester/polyethylene terephthalate, PUR: polyurethane, PCL: polycaprolactone, EVA: ethylene vinyl acetate.

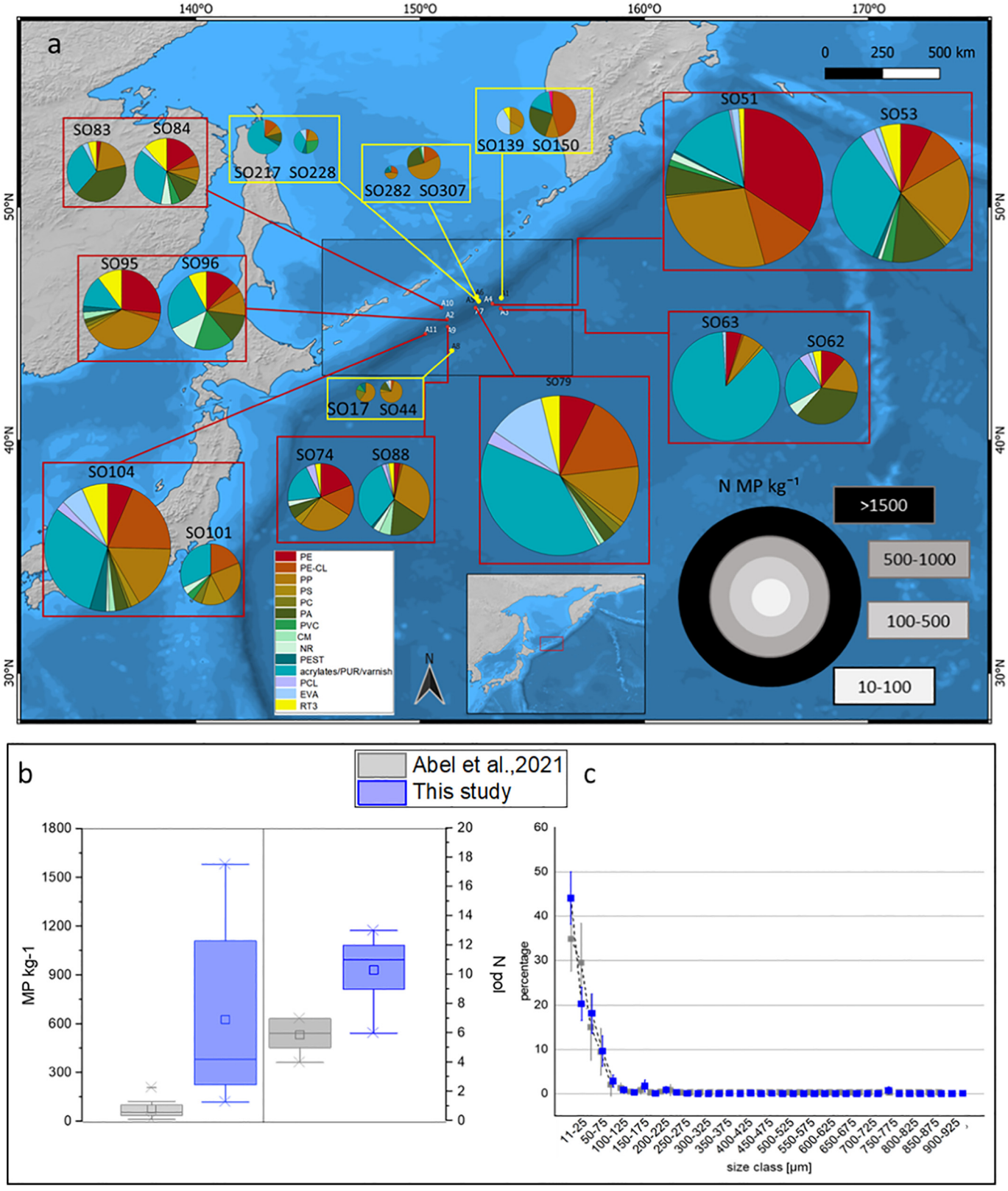

Fig. 4. (a): Comparison between the geographic distribution of sampling sites within the Kuril Kamchatka trench, sediment microplastic (MP) concentrations and relative polymer compositions, from the current study (red boxes) and those of Abel et al. (2021) (yellow boxes). MP concentration is reported in particles per kg sediment (DW), represented by the pie charts sizes. PE: polyethylene, PP: polypropylene, PS: polystyrene, PC: polycarbonate, PA: polyamide, PVC: polyvinyl chloride, PEST: polyester/polyethylene terephthalate, PUR: polyurethane, EVA: ethylene vinyl acetate. (b): Boxplots recording microplastic concentration (MP Kg^{-1}) and polymer diversity (N Pol) of both studies, grey box plots depict the outcomes of Abel et al., 2021, violet the outcomes from this study. (c): Comparison of the mean percentage of each size class in µm, for all sediment samples (squares), of both studies. Error bars show the 95% confidence interval.

4.4. Factors influencing the recovery efficiency

In most of analytical procedures, MP particles loss during laboratory processing can't be excluded completely, (Mani et al., 2019; Stock et al., 2022) nor the recovery rates of test particles, added to a sample, guarantees the same recovery efficiency of a procedure for environmental MP (Rozman and Kalčíková, 2022; Way et al., 2022). Effective methods for MP extraction from sediment matrixes depends on the reagents used (Quinn et al., 2017), the soil characteristics (Radford et al., 2021) including organic material content (Hurley et al., 2018), grain size (Möller et al., 2020) and the characteristics of the targeted MP (Horton et al., 2017). Therefore, recovery rates comparisons of different procedures must be reasonably contextualized and are informative if referred to similar sediment matrixes. Compared to the study conducted by Abel et al. (2021), on hadal samples collected in the KKT, in this study MP abundancies were 88% higher, confirming a lower particle loss during laboratory procedure. Nevertheless, without knowing the absolute value of MP at the trench floor, and given the heterogeneous distribution of MP in the samples, the MP load may be underestimated.

4.5. Processing procedure suitability

By comparing the MP concentrations detected in this study with those of the earlier study, both based on the identification of MP at the trench floor, important considerations regarding the analytical approach, in particular the processing of MP from the mineral matrix, are raised. Primarily, the discrepancies in MP concentrations between the two studies revealed that a MP processing method targeting a lower size class range, leads to a higher total MP recovery. In this study, the processing method tailored for reducing any potential particle loss caused by intrinsic set up proprieties and took into consideration the uniqueness of each sample during its analysis.

The outcomes of a previous study (Abel et al., 2021) were mandatory to establish the kind of contamination in terms of MP size and polymer composition (Möller et al., 2020), and set the bases for adequate processing procedure setup, given the uniqueness and little knowledge of the hadal sea floor. The suitability of an analytical procedure for MP analysis strongly depends on the research question. If the aim of an analysis, like in this study, is a precise MP investigation using a relatively low amount of sediment, a sample size conforming set-up that prioritises the reduction of particle loss, is recommended.

For a good representation of MP contamination in the environment, in this case the abyssal and hadal KKT floor, an adequate number of samples must be analysed in order to avoid misinterpretation deriving from the heterogeneous distribution of MP in environmental samples (Möller et al., 2020). The time required for the MP processing form a sediment matrix was therefore optimised to permit the analysis of a large sample numbers in short times, being at the same time reliable and accurate (Hengstmann and Fischer, 2019). Compared to previous MP processing procedures based on density separation (Bergmann et al., 2017a; Haave et al., 2019; Trinh et al., 2021) which required a setup of up to 24 h per sample, the procedure presented in this study allowed the processing of seven samples simultaneously within this time. This method is therefore compelling for research activities involved in MP monitoring in sediment matrices as it combines a simultaneous analysis of samples with a good representation of MP contamination, permitting a representative sampling of a non-homogeneously distributed particulate contaminant.

4.6. MP in the KKT

4.6.1. MP size classes

By considering the granulometry data of sediment cores sampled simultaneously in the same location of the cores analysed in this study (Aksentov and Sattarova, 2020), with the grain size range of the trench floor sediment (clay and silt, 0.98 and 62.5 μm respectively) and comparing this to the detected MP size range, with 94% of all MP particles being <75 μm, there is a clear match. It is plausible to assume that the "physical sedimentology" according to the definition provided by Allen (1985), can be applied to MP in the same way as for the sediment. The high amount of diatomaceous material and TOC (Kolesnik et al., 2019; Aksentov and Sattarova, 2020), as fractions of the sediment composition, is a further point of comparison given their comparable densities, thus the comparison of MP with organic matter and diatom frustules, in terms of their sedimentation behaviour, is particularly compelling (Harris, 2020).

The polymer composition detected in the sediment is diverse and includes both high- and low-density MP polymers. With low-density polymers being detected in all sediment samples and at every sediment column depth, this suggests that there are multiple pathways with which MP reaches the trench floor, including those pathways that lead to MP with neutral or positive buoyancies to sink.

A heterogeneous distribution of MP, in the sediment column and between different sampling stations, suggest that the localised sedimentation dynamics in the different areas of the trench influences the accumulation potential of MP.

Differences in MP concentration and polymer diversity through the sediment column in samples collected in the same area, suggests the occurrence of events that influence the sedimentation/resuspension dynamics in the range of meters, such as bioturbation and vorticity and are described further in detail later. A certain level of sampling disturbance, caused by the MUC of the first sampling event on the second, is not to be excluded as a sediment recasting factor (Underwood et al., 2017). Especially in the upper layers, the generally fine-grained sediment of the trench is easily susceptible to resuspension. To minimize the influence of this factor on the data interpretation, resuspended material present in the MUC core, as the fraction that is most likely disturbed by the sampling event, was not included in the evaluation of the MP composition of the samples, but was compared, for consistency, with the surface layer (0–1 cm). From this, it was possible to quantify the eventual loss, in terms of particle number and polymer diversity contribution, because of this exclusion (see SI).

4.6.2. Contextualisation of MP sedimentation dynamics within the KKT depositional system

The hadal region is one of the most challenging environments to study, given its remoteness and the difficult, time consuming and expensive sampling techniques required. MP pollution in the deepest trenches worldwide has, nevertheless, been reported, and defined hadal trenches as "the trash bins of the oceans" (Abel et al., 2021; Peng et al., 2020; Jamieson et al., 2019a; Peng et al., 2018a). Despite the certainty of the accumulation of MP in the trenches, the driving sedimentation dynamics at hadal depths remain relatively unclear. The unique topography of this environment, the consequently complex hydro-dynamical systems and sedimentation dynamics, together with challenging research conditions, make it difficult to clarify these processes.

It is also important to remark that hadal seafloor zones are not only influenced by topography, but also by the overlaying pelagic environment, their geographic position, oceanic currents, regional hydrodynamic conditions and seasonal events, such as algal blooms and river plumes consequent to massive seasonal rainfall, making the direct comparison between individual trenches difficult.

This study focuses on the complexity of the KKT sedimentary system, and the variability of its environmental signal. The latter term is meant as the changes in sediment production, transport, or deposition, which originate from environmental perturbations and is reflected in the MP distribution in sediment layers in different areas of the KKT (Romans et al., 2016). To study MP accumulation in the trench, it is essential to consider the entirety of factors that influences the sedimentation of material and supplies the sedimentary system of the trench, including sources, transport, and recast of sediment (summarized schematically in Fig. 5).

4.6.3. High productivity of the overlaying Pacific Subarctic Gyre region

The high biodiversity in the KKT is the consequence of a high POM (particulate organic matter) and POC (particulate organic carbon) flux driven by the overlaying biogeochemical province (Stewart and

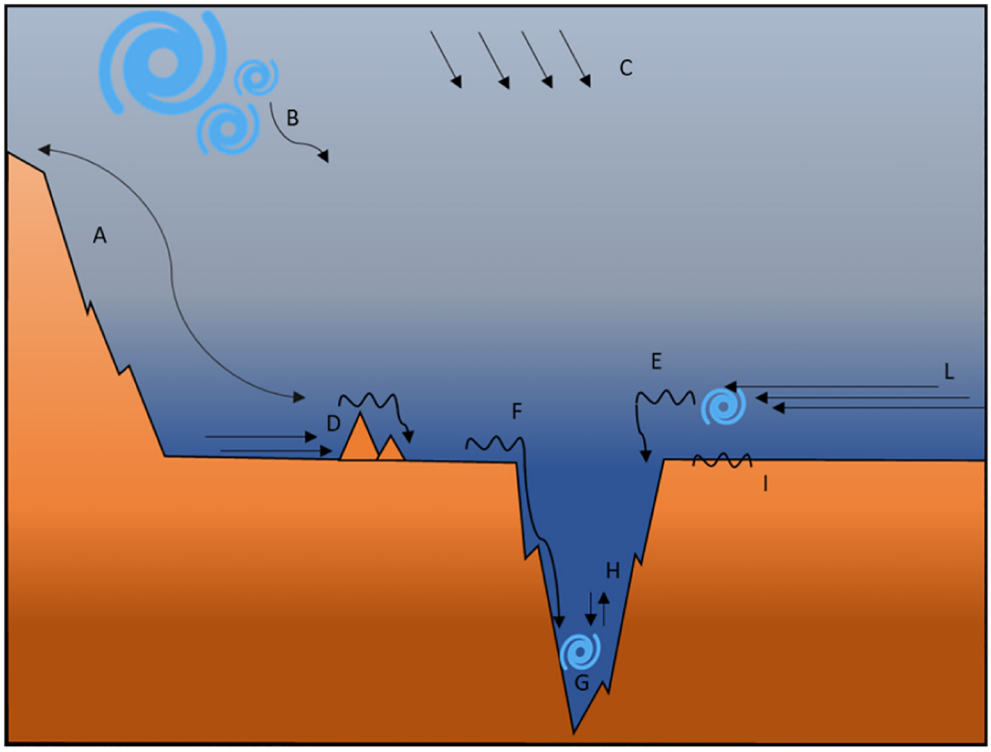

Fig. 5. Factors that influence the sedimentation of material and supplies the sedimentary system of the trench. A: Turbidity currents; B: Diapycnal mixing; C: Downfall; D: Laminar flow interruptions; E: Oceanic lee waves; F: Landslides on the trench slope G: Internal currents and vorticity; H: Recasting events in the trench; I: Bioturbation; L: Laminar flow.

Jamieson, 2018), thus, in terms of energy supply in form of nutrients, the trench is considered highly dynamic rather than stagnant (van Haren et al., 2017). The accumulation of POM in the trench is guaranteed by turbulent motions and gravity driven downward transport along the trench axis and these are considered the main driving forces for this transport (Danovaro et al., 2003; Jamieson, 2015; Otosaka and Noriki, 2000; Romankevich et al., 2009). On the one hand, these conditions sustain hadal life, but on the other hand, they also drive MP accumulation down to the deepest part of the trench.

By considering the province primary production rate of the Pacific Subarctic Gyre (PP PSAG: 264 g C m^{-2} yr^{-1}), the mean POC flux (2.26 ± 0.77 g C m^{-2} yr^{-1} ± S.D.) and total POC flux of the KKT (3118.86 g C yr^{-1}) against those rates and fluxes from other major subduction trenches, >6500 m depth, only two out of the 21 trenches are shown to be higher (Stewart and Jamieson, 2018). It is then clear that this trench receives a relatively high amount of POM compared to the other trenches (Longhurst, 2010). The aggregation of POM in marine snow increases the sedimentation velocity of material down to the trench, and concurs to the sequestration of MP in the sediment (Kvale et al., 2020b). This sedimentary input is temporally irregular, as the primary production and the resulting nutrients in the forms of POM and POC, from euphotic zones, is strongly seasonal. Assuming a close relationship between organic input and MP input into the KKT, the variable POM sedimentation rate may also help to explain the heterogeneous vertical and horizontal distribution of MP in the trench sediment.

4.6.4. Influence of the adjacent island arc

The Bussol Strait (2400 m) and the Krusenstern Strait (1500 m) (Fig. 1) are the two deepest straits that are connecting the Sea of Okhotsk and the North Pacific. The transport and mixing processes taking place between these two waterbodies, via the Kuril straits, play an important role not only in the local environment but also in determining the water properties of the North Pacific (Kitani, 1973). Nakamura and Awaji (2004), suggested the formation of large-amplitude unsteady lee waves that are generated around sill tops all along the Kuril Island Chain. These waves induce an enhanced diapycnal mixing and consequently create a significant density inversion from the sea surface down to deeper layers. Moreover, tidally induced baroclinic processes are responsible for low temperature anomalies, which indicate the formation of temperature fronts and eddies and are associated with vertical mixing and stirring (Simpson, 1997). By moving outwards, close to the trench and away from the turbulence source, suspended particles are no longer subjected to these events and settle, making the trench prone to sedimentation (Allen, 2012). Oceanic lee waves can also be generated in the deep stratified ocean by the flow of ocean currents over an uneven sea floor topography, like those characteristic of the trench edges (Nakamura et al., 2000). When the waves break, they can lead to mixing events in the stably stratified ocean interior (Legg, 2021). They can also interrupt the lateral advection of fine sediment and nepheloid layers close to the ocean floor, by altering the thermohaline circulation and cause contourite drifts. These are described by Kane and Clare, (2019b) and Kane et al. (2020) as one of the most important transport processes of fine-grained particles, including MP, in the deep sea.

Deep-sea circulation also influences the deposition and resuspension of MP on the seafloor, with bottom currents interacting with the seafloor and reworking the sediment and any MP present, in gravity flow systems and sequestering them within drift deposits (Rebesco et al., 2014). The granulometry of these deposits is characterised by fine grained, clay-silt sediment, similar to the sediment characterising the seafloor of the KKT, suggesting that this trench could be a conspicuous depocenter for these drift deposits.

4.6.5. Canyons and turbidites

The KKT sedimentary system is connected to a large submarine canyon system on the continental slope of Kamchatka. The scale of the individual canyons that make up this system range from the 40 km long Storozh Canyon, to the 175 km long Kamchatsky Canyon. Three of the canyons within the system (the Kamchatka, Zhupanovsky and Avachinsky canyons)

extend across the entire continental slope to the KKT, where they deposit their sediment (Gnibidenko and Svarichevskaya, 1984).

Submarine canyons consistently influence the sedimentation dynamics in deep sea trenches. Recently, Pohl et al. (2020) described submarine canyons as sites of preferential macroplastic and MP accumulation. When sampling these canyons, they detected double the MP concentration than was found in open slope continental shelve and abyssal plain sites. Furthermore, submarine canyons are described as conduits for gravity- driven avalanches of turbidity currents, highly efficient agents for transferring sediment and organic carbon from shallow to deep water (Galy et al., 2007; Liu, 2015). These currents are able to bury high proportions of the MP that they carry and to transport MP particles in distal lobe deposits. Large submarine canyons funnel coarse terrigenous debris directly to the trench floor, which effectively bypasses depositional sites along the lower slope (Underwood and Karig, 1980), and contributes to the transport of MP to the deepest parts of the trenches.

The predominance of a fine-grained fraction, the presence of turbidites in the upper sediment layers, and a higher MP concentration in the deeper sampling stations (A4, A11 and A7, Fig. 1) of the KKT, are evidence that the afore described dynamics are likely involved in sediment transport and its deposition within the KKT system.

4.6.6. Recasting events in the trench

Downfall alone cannot fully explain the heterogeneous distribution of MP in the trench and its depositional behaviour within the sediment depth profile. Once deposition of sediment occurs, perturbations such as earthquakes, submarine landslides (Kioka et al., 2019), internal currents (Turnewitsch et al., 2014), bioturbation by the local fauna (Brandt et al., 2015; Kamenev, 2019; Brandt et al., 2018; Bober et al., 2019; Błażewicz-Paszkowycz et al., 2015; Malyutina and Brandt, 2020; Fukumori et al., 2019; Brandt et al., 2019) and location-specific hydrography can rework the sediment layers and depositional processes on different scales of magnitude.

4.6.7. Location dependent factors

Highly heterogeneous environmental features, including avalanche deposits, internal hills, canyons and depressions, reflect the highly heterogeneous MP distribution within the sediment depth profiles and between sampling locations within the KKT. By observing the distribution of MP throughout the sediment profile, the relative distributions of MP in the samples are consistently different from each other, implying variations in resuspension and burial factors. In highly dynamic areas, fine and superficial particles are continuedly resuspended and transported elsewhere, therefore making the deposition and/or burial of these particles difficult. This resuspension activity may be translated to a low MP load in the sediment profile in general and a reduction of MP distribution in the deeper layers and can be observed, for example, in the samples from stations A9 and A10 (Fig. 3). The opposite trend was observed in areas with weak hydrodynamics, with high quantities of MP expected due to the tendency for MP accumulation, including in the surface sediment layer, as was the case for station A7.

These two distribution trends can be considered as a simplified situation, in which no other confounding factors are contributing to the dispersion of MP in the sediment and where the hydrodynamic conditions are consistently stable. When only considering the mean annual deposition rate within the KKT (1.3 mm/year) (Aksentov and Sattarova, 2020), the first 5 cm of sediment would have been deposited over the last 65 years, however, within this timeframe, the local topography is likely to have been reshaped by the afore mentioned large- and small-scale hydrodynamic perturbation events, therefore altering the homogeneity of sediment and MP deposition within the trench.

Assuming that location-specific hydrodynamics are the main factors driving MP sedimentation trends, an increase in high-energy turbulent conditions would lead to a decrease in MP accumulation, and vice-versa, with a higher MP accumulation expected with decreasing turbulence.

By considering in the sampled locations at station A10, A3, A2 and A9 (trends are visible in Fig. 3, to visualise the location of the station, consult Fig. 1), the MP accumulation trends show low MP concentrations, which reflects high energetic locations, in which MP do not readily accumulate. Stations A4 and A7, however, appear to show an affinity for the accumulation of MP, possibly due to the presence of less energetic hydrological conditions. Focusing on the distribution of MP in the sediment column, the accumulation trends (Fig. 3) suggest that local fluctuations in hydrodynamic conditions lead to fluctuations in sedimentation patterns, depending, among other reasons, on the specific area and its topographic variability.

When evaluating MP accumulation trends through the sediment depth profile, factors, including hydrodynamics, have to be taken in consideration, especially when comparing sediment cores collected in the same location. The MP accumulation trends of A9 and A4 (Fig. 3), for example, could reflect a highly dynamic event succession. Both cores from station A9 (SO74 and SO88) have low total MP concentrations, but the distribution of the MP that are present in the two sediment columns are distinctly different. In A9, core SO74 has a relatively high MP number in the surface layer, but with relatively low numbers of MP detected in the rest of the profile. Taken from the same station, core SO88, shows a succession of low to relatively high MP concentrations through the sediment profile. In A4, both cores (SO51 and SO53) have a relatively high concentration of MP, with alternating layers of higher and lower MP content, but with an inverted trend. In this location, local vorticity may act on the sedimentation and resuspension of particles, avalanches could have shifted the deposited layers and bioturbation is likely to have recasts the sediment column to some degree.

By comparing the cores in A11 (SO101 and S104) and A3 (core SO62 and SO63), an uneven distribution of MP in the sediments is evident in terms of concentration and polymer composition. This heterogeneous distribution of MP in the sediment of the KKT can therefore be classified as a stochastic factor (Fisner et al., 2017; Martin et al., 2017; Nuelle et al., 2014).

Statistical analysis by Pearson correlation revealed a positive correlation between the sampling station depth and MP concentration ($r = 0.311$, $p = 0.0117$). A similar trend was also observed in a recent study carried out on other sediment samples taken from the KKT, in which MP concentrations were also higher in the deeper stations (Abel et al., 2021). Premising the non-absolutistic value of this assumption, due to the impossibility of limited sampling representing such a vast, inaccessible and heterogeneous environment, as a hadal trench, with complete accuracy, the outcomes of both studies, nevertheless, seem to validate the hypothesis that the deepest part of the trench is a region polluted with MP, if not the most polluted. This validation leads back to the significance of gravitational effects, with the hadal floor, at its deepest part, being the end destination of many MP transport pathways, such as sinking from the water column and downslope transport.

5. Conclusion

This study focused on improving our understanding of the MP sedimentation in the context of deep-sea depositional system dynamics. Our results highlight, firstly, that there is a heterogeneous distribution of MP between locations within the KKT, likely resulting from the dynamic environment of this hadal trench; and secondly, that MP heterogeneity within the sediment profile reflects the site-specific hydrodynamic conditions and the local sediment recasting events. The first was confirmed by consistent differences in MP concentration and polymer composition in sediment collected from different areas of the trench. The second led from differences in cores collected at the same sampling station only a few meters apart and from stochastic trends of MP distribution through the sediment column. Overall, MP numbers in this study exceeded those of previous assessments of the KKT by one order of magnitude. The applied method permitted a higher detection of MP belonging to the lower size range and revealed a greater level of MP contamination on the seafloor of the KKT than was known previously.

CRediT authorship contribution statement

Serena M. Abel: Writing – original draft, Writing – review & editing, Visualization, Formal analysis, Methodology, Investigation. **Sebastian**

Primpke: Software, Writing – review & editing. **Fangzhu Wu:** Investigation, Writing – review & editing. **Angelika Brandt:** Project administration, Writing – review & editing. **Gunnar Gerdts:** Supervision, Formal analysis, Resources, Writing – review & editing.

Declaration of competing interest

The authors declare that they have no known competing financial interests or personal relationships that could have appeared to influence the work reported in this paper.

Acknowledgments

The material was collected and sorted within the framework of the KuramBio II project supported by the PTJ (German Ministry for Science and Education, BMBF grant 03G0250A) to Prof. Dr. Angelika Brandt, Senckenberg Museum, and Goethe University Frankfurt, Germany. We thank the crew of the RVs *Sonne* for their help on board. Furthermore, we thank Nicholas Jamie Mackay-Roberts and Clara Leistenschneider for proof-reading of the manuscript.

Appendix A. Supplementary data

Supplementary data to this article can be found online at https://doi.org/10.1016/j.scitotenv.2022.156035.

References

Abel, S.M., Primpke, S., Int-Veen, I., Brandt, A., Gerdts, G., 2021. Systematic identification of microplastics in abyssal and hadal sediments of the Kuril Kamchatka trench. Environ. Pollut. 269, 116095.

Aksentov, K.I., Sattarova, V.V., 2020. Mercury geochemistry of deep-sea sediment cores from the Kuril area, northwest Pacific. Prog. Oceanogr. 180, 102235.

Allen, J., 1985. Sink or swim? Principles of Physical Sedimentology. Springer, pp. 39–54

Allen, J., 2012. Principles of Physical Sedimentology. Springer Science & Business Media.

Andrady, A.L., 2011. Microplastics in the marine environment. Mar. Pollut. Bull. 62, 1596–1605.

Avdeiko, G., Savelyev, D., Palueva, A., Popruzhenko, S., 2007. Evolution of the Kurile-Kamchatkan volcanic arcs and dynamics of the Kamchatka-Aleutian junction. Geophys. Monogr.-Am. Geophys. Union 172, 37.

Bergmann, M., Wirzberger, V., Krumpen, T., Lorenz, C., Primpke, S., Tekman, M.B., Gerdts, G., 2017a. High quantities of microplastic in Arctic Deep-Sea sediments from the HAUSGARTEN observatory. Environ. Sci. Technol. 51, 11000–11010.

Bergmann, M., Wirzberger, V., Krumpen, T., Lorenz, C., Primpke, S., Tekman, M.B., Gerdts, G., 2017b. High quantities of microplastic in Arctic Deep-Sea sediments from the HAUSGARTEN Observatory. Environ. Sci. Technol. 51, 11000–11010.

Bergmann, M., Mützel, S., Primpke, S., Tekman, M.B., Trachsel, J., Gerdts, G., 2019. White and wonderful? Microplastics prevail in snow from the Alps to the Arctic. Sci.Adv. 5, eaax1157.

Błażewicz-Paszkowycz, M., Pabis, K., Jóźwiak, P., 2015. Tanaidacean fauna of the Kuril-Kamchatka Trench and adjacent abyssal plain – abundance, diversity and rare species. Deep-Sea Res. II Top. Stud. Oceanogr. 111, 325–332.

Bober, J., Brandt, A., Frutos, I., Schwentner, M., 2019. Diversity and distribution of ischnomesidae (Crustacea: Isopoda: Asellota) along the Kuril-Kamchatka Trench – a genetic perspective. Prog. Oceanogr. 178, 102174.

Braitseva, O.A., Melekestsev, I.V., Ponomareva, V.V., Sulerzhitsky, L.D., 1995. Ages of calderas, large explosive craters and active volcanoes in the Kuril-Kamchatka region, Russia. Bull. Volcanol. 57, 383–402.

Brandt, A., Elsner, N.O., Malyutina, M.V., Brenke, N., Golovan, O.A., Lavrenteva, A.V., Riehl, T., 2015. Abyssal macrofauna of the Kuril-Kamchatka Trench area (Northwest Pacific) collected by means of a camera–epibenthic sledge. Deep-Sea Res. II Top. Stud. Oceanogr. 111, 175–187.

Brandt, A., Alalykina, I., Fukumori, H., Golovan, O., Kniesz, K., Lavrenteva, A., Lörz, A.N., Malyutina, M., Philipps-Bussau, K., Stransky, B., 2018. First insights into macrofaunal composition from the SokhoBio expedition (Sea of Okhotsk, Bussol Strait and northern slope of the Kuril-Kamchatka Trench). Deep-Sea Res. II Top. Stud. Oceanogr. 154, 106–120.

Brandt, A., Alalykina, I., Brix, S., Brenke, N., Błażewicz, M., Golovan, O.A., Johannsen, N., Hrinko, A.M., Jażdżewska, A.M., Jeskulke, K., Kamenev, G.M., Lavrenteva, A.V., Malyutina, M.V., Riehl, T., Lins, L., 2019. Depth zonation of Northwest Pacific deep-sea macrofauna. Prog. Oceanogr. 176, 102131.

Bucol, L.A., Romano, E.F., Cabcaban, S.M., Siplon, L.M.D., Madrid, G.C., Bucol, A.A., Polidoro, B., 2020. Microplastics in marine sediments and rabbitfish (Siganus fuscescens) from selected coastal areas of Negros Oriental,Philippines. Mar. Pollut. Bull. 150, 110685.

Cashman, M.A., Ho, K.T., Boving, T.B., Russo, S., Robinson, S., Burgess, R.M., 2020. Comparison of microplastic isolation and extraction procedures from marine sediments. Mar. Pollut. Bull. 159, 111507.

Cincinelli, A., Martellini, T., Guerranti, C., Scopetani, C., Chelazzi, D., Giarrizzo, T., 2019. A potpourri of microplastics in the sea surface and water column of the Mediterranean Sea. TrAC Trends Anal. Chem. 110, 321–326.

Coppock, R.L., Cole, M., Lindeque, P.K., Queirós, A.M., Galloway, T.S., 2017. A small-scale, portable method for extracting microplastics from marine sediments. Environ. Pollut. 230, 829–837.

Courtene-Jones, W., Quinn, B., Gary, S.F., Mogg, A.O., Narayanaswamy, B.E., 2017. Microplastic pollution identified in deep-sea water and ingested by benthic invertebrates in the Rockall Trough, North Atlantic Ocean. Environ. Pollut. 231, 271–280.

Cózar, A., Echevarría, F., González-Gordillo, J.I., Irigoien, X., Úbeda, B., Hernández-León, S., Palma, Á.T., Navarro, S., García-de-Lomas, J., Ruiz, A., Fernández-de-Puelles, M.L., Duarte, C.M., 2014. Plastic debris in the open ocean. Proc. Natl. Acad. Sci. 111, 10239.

Dai, Z., Zhang, H., Zhou, Q., Tian, Y., Chen, T., Tu, C., Fu, C., Luo, Y., 2018. Occurrence of microplastics in the water column and sediment in an inland sea affected by intensive anthropogenic activities. Environ. Pollut. 242, 1557–1565.

Danovaro, R., Della Croce, N., Dell'Anno, A., Pusceddu, A., 2003. A depocenter of organic matter at 7800m depth in the SE Pacific Ocean. Deep-Sea Res. I Oceanogr. Res. Pap. 50, 1411–1420.

Filgueiras, A.V., Gago, J., García, I., León, V.M., Viñas, L., 2021. Plackett Burman design for microplastics quantification in marine sediments. Mar. Pollut. Bull. 162, 111841.

Fischer, K.M., Yang, X., 1994. Anisotropy in Kuril-Kamchatka subduction zone structure. Geophys. Res. Lett. 21, 5–8.

Fisner, M., Majer, A.P., Balthazar-Silva, D., Gorman, D., Turra, A., 2017. Quantifying microplastic pollution on sandy beaches: the conundrum of large sample variability and spatial heterogeneity. Environ. Sci. Pollut. Res. 24, 13732–13740.

Fukumori, H., Takano, T., Hasegawa, K., Kano, Y., 2019. Deepest known gastropod fauna: species composition and distribution in the Kuril-Kamchatka Trench. Prog. Oceanogr. 178, 102176.

Galy, V., France-Lanord, C., Beyssac, O., Faure, P., Kudrass, H., Palhol, F., 2007. Efficient organic carbon burial in the Bengal fan sustained by the Himalayan erosional system. Nature 450, 407–410.

Gnibidenko, H.S., Svarichevskaya, L.V., 1984. The submarine canyons of Kamchatka. Mar. Geol. 54, 277–307.

Golovan, O.A., Błażewicz, M., Brandt, A., Jażdżewska, A.M., Jóźwiak, P., Lavrenteva, A.V., Malyutina, M.V., Petryashov, V.V., Riehl, T., Sattarova, V.V., 2019. Diversity and distribution of peracarid crustaceans (Malacostraca) from the abyss adjacent to the Kuril-Kamchatka Trench. Mar. Biodivers. 49, 1343–1360.

Haave, M., Lorenz, C., Primpke, S., Gerdts, G., 2019. Different stories told by small and large microplastics in sediment-first report of microplastic concentrations in an urban recipient in Norway. Mar. Pollut. Bull. 141, 501–513.

van Haren, H., Berndt, C., Klaucke, I., 2017. Ocean mixing in deep-sea trenches: new insights from the challenger deep, Mariana trench. Deep-Sea Res. I Oceanogr. Res. Pap. 129, 1–9.

Harris, P.T., 2020. The fate of microplastic in marine sedimentary environments: a review and synthesis. Mar. Pollut. Bull. 158, 111398.

Hengstmann, E., Fischer, E.K., 2019. Nile red staining in microplastic analysis—proposal for a reliable and fast identification approach for large microplastics. Environ. Monit. Assess. 191, 612.

Horton, A.A., Svendsen, C., Williams, R.J., Spurgeon, D.J., Lahive, E., 2017. Large microplastic particles in sediments of tributaries of the River Thames, UK – abundance, sources and methods for effective quantification. Mar. Pollut. Bull. 114 (1), 218–226.

Hurley, R.R., Lusher, A.L., Olsen, M., Nizzetto, L., 2018. Validation of a method for extracting microplastics from complex, organic-rich, environmental matrices. Environ. Sci. Technol. 52, 7409–7417.

Imhof, H.K., Schmid, J., Niessner, R., Ivleva, N.P., Laforsch, C., 2012a. A novel, highly efficient method for the separation and quantification of plastic particles in sediments of aquatic environments. Limnol. Oceanogr. Methods 10, 524–537.

Imhof, H.K., Schmid, J., Niessner, R., Ivleva, N.P., Laforsch, C., 2012b. A novel, highly efficient method for the separation and quantification of plastic particles in sediments of aquatic environments. Limnol. Oceanogr. Methods 10, 524–537.

Jamieson, A., 2015. The Hadal Zone: Life in the Deepest Oceans. Cambridge University Press.

Jamieson, A., Brooks, L., Reid, W., Piernteyy, S., Narayanaswamy, B., Linley, T., 2019a. Microplastics and synthetic particles ingested by deep-sea amphipods in six of the deepest marine ecosystems on Earth. R. Soc. Open Sci. 6, 180667.

Jamieson, A.J., Brooks, L., Reid, W.D., Piertney, S., Narayanaswamy, B.E., Linley, T., 2019b. Microplastics and synthetic particles ingested by deep-sea amphipods in six of the deepest marine ecosystems on Earth. R. Soc. Open Sci. 6, 180667.

Kalak, T., 2018. Responsibility for Marine Litter Floating in the North Pacific Ocean.

Kamenev, G.M., 2019. Bivalve mollusks of the Kuril-Kamchatka Trench, Northwest Pacific Ocean: species composition, distribution and taxonomic remarks. Prog. Oceanogr. 176, 102127.

Kane, I.A., Clare, M.A., 2019a. Dispersion, accumulation, and the ultimate fate of microplastics in deep-marine environments: a review and future directions. Front. Earth Sci. 7, 80.

Kane, I.A., Clare, M.A., Miramontes, E., Wogelius, R., Rothwell, J.J., Garreau, P., Pohl, F., 2020. Seafloor microplastic hotspots controlled by deep-sea circulation. Science 368, 1140–1145.

Kelly, A., Lannuzel, D., Rodemann, T., Meiners, K., Auman, H., 2020. Microplastic contamination in east Antarctic sea ice. Mar. Pollut. Bull. 154, 111130.

Kioka, A., Schwestermann, T., Moernaut, J., Ikehara, K., Kanamatsu, T., Eglinton, T.I., Strasser, M., 2019. Event stratigraphy in a hadal oceanic trench: the Japan trench as sedimentary archive recording recurrent giant subduction zone earthquakes and their role in organic carbon export to the deep sea. Front. Earth Sci. 7, 319.

Kitani, K., 1973. An oceanographic study of the Okhotsk Sea-particularly in regard to cold waters. Bull. Far. Seas Fish. Res. 9, 45–77.

Klovach, N., Leman, V., Gordeev, I., 2021. The relative importance of enhancement to the production of Salmon on Iturup Island (Kuril Islands, Russia). Rev. Aquac. 13, 664–675.

Kolesnik, A.N., Kolesnik, O.N., Sattarova, V.V., Karabtsov, A.A., Yaroshchuk, E.I., 2019. Color and chemical composition of bottom sediments from the Kuril Basin (Sea of Okhotsk) and the Kuril-Kamchatka Trench area (Northwest Pacific). Prog. Oceanogr. 178, 102197.
Kvale, K.F., Friederike Prowe, A., Oschlies, A., 2020a. A critical examination of the role of marine snow and zooplankton fecal pellets in removing ocean surface microplastic. Front. Mar. Sci. 6, 808.
Kvale, K.F., Friederike Prowe, A.E., Oschlies, A., 2020b. A critical examination of the role of marine snow and zooplankton fecal pellets in removing ocean surface microplastic. Front. Mar. Sci. 6.
La Daana, K.K., Gardfeldt, K., Krumpen, T., Thompson, R.C., O'Connor, I., 2020. Microplastics in sea ice and seawater beneath ice floes from the Arctic Ocean. Sci. Rep. 10, 1–11.
Lebreton, L., Van Der Zwet, J., Damsteeg, J.-W., Slat, B., Andrady, A., Reisser, J., 2017. River plastic emissions to the world's oceans. Nat. Commun. 8, 1–10.
Legg, S., 2021. Mixing by oceanic lee waves. Annu. Rev. Fluid Mech. 53, 173–201.
Liu, J., 2015. From the highest to the deepest: the Gaoping River-Gaoping Submarine Canyon dispersal system. Earth Sci. Rev. 153.
Liu, M., Song, Y., Lu, S., Qiu, R., Hu, J., Li, X., Bigalke, M., Shi, H., He, D., 2019. A method for extracting soil microplastics through circulation of sodium bromide solutions. Sci. Total Environ. 691, 341–347.
Longhurst, A.R., 2010. Ecological Geography of the Sea. Elsevier.
Lorenz, C., 2014. Detection of microplastics in marine sediments of the German Coast via FT-IR spectroscopy. Applied Ecology and Phycology. Universität Rostock, Rostock, pp. 1–77.
Lorenz, C., Speidel, L., Primpke, S., Gerdts, G., 2016. Using the FlowCam to validate an enzymatic digestion protocol applied to assess the occurrence of microplastics in the Southern North Sea. MICRO 92–93.
Lorenz, C., Speidel, L., Primpke, S., Gerdts, G., 2017. Using the FlowCam to Validate an Enzymatic Digestion Protocol Applied to Assess the Occurrence of Microplastics in the Southern North Sea, Fate and Impact of Microplastics in Marine Ecosystems. Elsevier, pp. 92–93.
Lorenz, C., Schafberg, M., Roscher, L., Meyer, M.S., Primpke, S., Kraus, U.R., Gerdts, G., 2021. Paraffin and other petroleum waxes in the southern North Sea. Mar. Pollut. Bull. 162, 111807.
Mahat, S., 2017. Separation and Quantification of Microplastics From Beach and Sediment Samples Using the Bauta Microplastic-sediment Separator. Norwegian University of Life Sciences, Ås.
Malyutina, M.V., Brandt, A., 2020. Munnopsidae (Crustacea, Isopoda, Asellota) from the Kuril-Kamchatka Trench with a regional and inter-ocean comparison of their biogeographic and richness patterns. Prog. Oceanogr. 183, 102289.
Mani, T., Primpke, S., Lorenz, C., Gerdts, G., Burkhardt-Holm, P., 2019. Microplastic pollution in benthic midstream sediments of the Rhine River. Environ. Sci. Technol 53, 6053–6062.
Martin, J., Lusher, A., Thompson, R.C., Morley, A., 2017. The deposition and accumulation of microplastics in marine sediments and bottom water from the Irish Continental Shelf. Sci. Rep. 7, 10772.
Matsushita, K., Uchiyama, Y., Takaura, N., Kosako, T., 2021. Medium-Term Oceanic Transport of River-Derived Microplastics in the South China Sea Analyzed With a Particle Tracking Model. IOP Conference Series: Earth and Environmental Science. IOP Publishing, p. 012029.
Möller, J.N., Löder, M.G.J., Laforsch, C., 2020. Finding microplastics in soils: a review of analytical methods. Environ. Sci. Technol. 54, 2078–2090.
Nakajima, R., Tsuchiya, M., Yabuki, A., Masuda, S., Kitahashi, T., Nagano, Y., Ikuta, T., Isobe, N., Nakata, H., Ritchie, H., 2021. Massive occurrence of benthic plastic debris at the abyssal seafloor beneath the Kuroshio extension, the North West Pacific. Mar. Pollut. Bull. 166, 112188.
Nakamura, T., Awaji, T., 2004. Tidally induced diapycnal mixing in the Kuril Straits and its role in water transformation and transport: a three-dimensional nonhydrostatic model experiment. J. Geophys. Res. (Oceans) 109, C09S07.
Nakamura, T., Awaji, T., Hatayama, T., Akitomo, K., Takizawa, T., Kono, T., Kawasaki, Y., Fukasawa, M., 2000. The generation of large-amplitude unsteady lee waves by subinertial K1 tidal flow: a possible vertical mixing mechanism in the Kuril Straits. J. Phys. Oceanogr. 30, 1601–1621.
Näkki, P., Setälä, O., Lehtiniemi, M., 2017. Bioturbation transports secondary microplastics to deeper layers in soft marine sediments of the northern Baltic Sea. Mar. Pollut. Bull. 119, 255–261.
Nishizawa, B., Thiebot, J.-B., Sato, F., Tomita, N., Yoda, K., Yamashita, R., Takada, H., Watanuki, Y., 2021. Mapping marine debris encountered by albatrosses tracked over oceanic waters. Sci. Rep. 11, 1–7.
Nuelle, M.-T., Dekiff, J.H., Remy, D., Fries, E., 2014. A new analytical approach for monitoring microplastics in marine sediments. Environ. Pollut. 184, 161–169.
Obbard, R.W., 2018. Microplastics in polar regions: the role of long range transport. Curr. Opin. Environ. Sci. Health 1, 24–29.
Otosaka, S., Noriki, S., 2000. REEs and Mn/Al ratio of settling particles: horizontal transport of particulate material in the northern Japan Trench. Mar. Chem. 72, 329–342.
Peeken, I., Primpke, S., Beyer, B., Gütermann, J., Katlein, C., Krumpen, T., Bergmann, M., Hehemann, L., Gerdts, G., 2018. Arctic sea ice is an important temporal sink and means of transport for microplastic. Nat. Commun. 9, 1–12.
Peng, X., Chen, M., Chen, S., Dasgupta, S., Xu, H., Ta, K., Du, M., Li, J., Guo, Z., Bai, S., 2018a. Microplastics contaminate the deepest part of the world's ocean. Geochem. Perspect. Lett. 9, 1–5.
Peng, X., Chen, M., Chen, S., Dasgupta, S., Xu, H., Ta, K., Du, M., Li, J., Guo, Z., Bai, S., 2018b. Microplastics contaminate the deepest part of the world's ocean. Geochem. Perspect. Lett 9, 1–5.
Peng, G., Bellerby, R., Zhang, F., Sun, X., Li, D., 2020. The ocean's ultimate trashcan: hadal trenches as major depositories for plastic pollution. Water Res. 168, 115121.
Petersen, F., Hubbart, J.A., 2021. The occurrence and transport of microplastics: the state of the science. Sci. Total Environ. 758, 143936.
Pohl, F., Eggenhuisen, J.T., Kane, I.A., Clare, M.A., 2020. Transport and burial of microplastics in deep-marine sediments by turbidity currents. Environ. Sci. Technol. 54, 4180–4189.
Porter, A., Lyons, B.P., Galloway, T.S., Lewis, C., 2018. Role of marine snows in microplastic fate and bioavailability. Environ. Sci. Technol. 52, 7111–7119.
Primpke, S., Lorenz, C., Rascher-Friesenhausen, R., Gerdts, G., 2017. An automated approach for microplastics analysis using focal plane array (FPA) FTIR microscopy and image analysis. Anal. Methods 9, 1499–1511.
Primpke, S., Wirth, M., Lorenz, C., Gerdts, G., 2018. Reference database design for the automated analysis of microplastic samples based on fourier transform infrared (FTIR) spectroscopy. Anal. Bioanal. Chem. 410, 5131–5141.
Primpke, S., Dias, A.P., Gerdts, G., 2019. Automated identification and quantification of microfibres and microplastics. Anal. Methods 11, 2138–2147.
Primpke, S., Cross, R.K., Mintenig, S.M., Simon, M., Vianello, A., Gerdts, G., Vollertsen, J., 2020. Toward the systematic identification of microplastics in the environment: evaluation of a new independent software tool (siMPle) for spectroscopic analysis. Appl. Spectrosc. 74, 1127–1138.
Quinn, B., Murphy, F., Ewins, C., 2017. Validation of density separation for the rapid recovery of microplastics from sediment. Anal. Methods 9, 1491–1498.
Radford, F., Zapata-Restrepo, L.M., Horton, A.A., Hudson, M.D., Shaw, P.J., Williams, I.D., 2021. Developing a systematic method for extraction of microplastics in soils. Anal. Methods 13 (14), 1695–1705.
Rebesco, M., Hernández-Molina, F.J., Van Rooij, D., Wåhlin, A., 2014. Contourites and associated sediments controlled by deep-water circulation processes: state-of-the-art and future considerations. Mar. Geol. 352, 111–154.
Reed, S., Clark, M., Thompson, R., Hughes, K.A., 2018. Microplastics in marine sediments near Rothera research station, Antarctica. Mar. Pollut. Bull. 133, 460–463.
Romankevich, E.A., Vetrov, A.A., Peresypkin, V.I., 2009. Organic matter of the World Ocean. Russ. Geol. Geophys. 50, 299–307.
Romans, B.W., Castelltort, S., Covault, J.A., Fildani, A., Walsh, J.P., 2016. Environmental signal propagation in sedimentary systems across timescales. Earth Sci. Rev. 153, 7–29.
Roscher, L., Fehres, A., Reisel, L., Halbach, M., Scholz-Böttcher, B., Gerriets, M., Badewien, T.H., Shiravani, G., Wurpts, A., Primpke, S., 2021a. Microplastic pollution in the Weser estuary and the German North Sea. Environ. Pollut. 288, 117681.
Roscher, L., Halbach, M., Nguyen, M.T., Hebeler, M., Luschtinetz, F., Scholz-Böttcher, B.M., Primpke, S., Gerdts, G., 2021. Microplastics in two German wastewater treatment plants: year-long effluent analysis with FTIR and Py-GC/MS. Sci. Total Environ. 152619.
Rozman, U., Kalčíková, G., 2022. Seeking for a perfect (non-spherical) microplastic particle – the most comprehensive review on microplastic laboratory research. J. Hazard. Mater. 424, 127529.
Ryan, P.G., 2020. The transport and fate of marine plastics in South Africa and adjacent oceans. S. Afr. J. Sci. 116, 1–9.
Saito, H., 2019. The Kuroshio, pp. 1–11.
Sattarova, V.V., Aksentov, K.I., 2021. Trace metals in deep-sea sediments collected from Kuril Basin (Sea of Okhotsk) and kuril-Kamchatka trench area. Mar. Pollut. Bull. 164, 112055.
Schmidt, C., Krauth, T., Wagner, S., 2017. Export of plastic debris by rivers into the sea. Environ. Sci. Technol. 51, 12246–12253.
Shiu, R.-F., Gong, G.-C., Fang, M.-D., Chow, C.-H., Chin, W.-C., 2021. Marine microplastics in the surface waters of "pristine" kuroshio. Mar. Pollut. Bull. 172, 112808.
Simpson, J.H., 1997. Physical processes in the ROFI regime. J. Mar. Syst. 12, 3–15.
Steblov, G.M., Vasilenko, N.F., Prytkov, A.S., Frolov, D.I., Grekova, T.A., 2010. Dynamics of the kuril-Kamchatka subduction zone from GPS data,Izvestiya. Phys. Solid Earth 46, 440–445.
Stewart, H.A., Jamieson, A.J., 2018. Habitat heterogeneity of hadal trenches: considerations and implications for future studies. Prog. Oceanogr. 161, 47–65.
Stock, F., Kochleus, C., Bänsch-Baltruschat, B., Brennholt, N., Reifferscheid, G., 2019. Sampling techniques and preparation methods for microplastic analyses in the aquatic environment–A review. TrAC Trends Anal. Chem. 113, 84–92.
Stock, F., Narayana, V.K.B., Scherer, C., Löder, M.G.J., Brennholt, N., Laforsch, C., Reifferscheid, G., 2022. In: Stock, F., Reifferscheid, G., Brennholt, N., Kostianaia, E. (Eds.), Pitfalls and Limitations in Microplastic Analyses. Plastics in the Aquatic Environment - Part I: Current Status and Challenges. Springer International Publishing, Cham, pp. 13–42.
Tagg, A., Harrison, J., Ju-Nam, Y., Sapp, M., Bradley, E., Sinclair, C., Ojeda, J., 2017. Fenton's reagent for the rapid and efficient isolation of microplastics from wastewater. Chem. Commun. (Camb.) 53, 372–375.
Tekman, M.B., Krumpen, T., Bergmann, M., 2017. Marine litter on deep Arctic seafloor continues to increase and spreads to the north at the HAUSGARTEN observatory. Deep-Sea Res. I Oceanogr. Res. Pap. 120, 88–99.
Tekman, M.B., Wekerle, C., Lorenz, C., Primpke, S., Hasemann, C., Gerdts, G., Bergmann, M., 2020. Tying up loose ends of microplastic pollution in the Arctic: distribution from the sea surface through the water column to Deep-Sea sediments at the HAUSGARTEN observatory. Environ Sci Technol 54, 4079–4090.
Trinh, B.-S., Dam, V.N., Pham, B.L.T., Pham, H.C., 2021. A separation of plastic debris in Saigon river sediment using a microplastic sediment separator. Sci. Technol. Dev. J.-Sci. Earth Environ. 5, SI137–SI146.
Turnewitsch, R., Falahat, S., Stehlikova, J., Oguri, K., Glud, R.N., Middelboe, M., Kitazato, H., Wenzhöfer, F., Ando, K., Fujio, S., 2014. Recent sediment dynamics in hadal trenches: evidence for the influence of higher-frequency (tidal, near-inertial) fluid dynamics. Deep-Sea Res. I Oceanogr. Res. Pap. 90, 125–138.
Uehara, K., Miyake, H., 1999. Deep flows on the slope inshore of the Kuril-Kamchatka Trench southeast off Cape Erimo, Hokkaido. J. Oceanogr. 55, 559–573.
Underwood, M., Karig, D., 1980. Role of submarine canyons in trench and trench-slope sedimentation. Geology 8, 432–436.
Underwood, A., Chapman, M., Browne, M.A., 2017. Some problems and practicalities in design and interpretation of samples of microplastic waste. Anal. Methods 9, 1332–1345.
Way, C., Hudson, M.D., Williams, I.D., Langley, G.J., 2022. Evidence of underestimation in microplastic research: a meta-analysis of recovery rate studies. Sci. Total Environ. 805, 150227.

Witzig, C.S., Földi, C., Wörle, K., Habermehl, P., Pittroff, M., Müller, Y.K., Lauschke, T., Fiener, P., Dierkes, G., Freier, K.P., 2020. When good intentions go bad—false positive microplastic detection caused by disposable gloves. Environ. Sci. Technol. 54, 12164–12172.

Yagi, M., Yasuda, I., 2012. Deep intense vertical mixing in the Bussol'Strait. Geophys. Res. Lett. 39.

Yagi, M., Yasuda, I., 2013. A modified method for estimating vertical profiles of turbulent dissipation rate using density inversions in the Kuril Straits. J. Oceanogr. 69, 203–214.

Zhang, D., Liu, X., Huang, W., Li, J., Wang, C., Zhang, D., Zhang, C., 2020. Microplastic pollution in deep-sea sediments and organisms of the Western Pacific Ocean. Environ. Pollut. 259, 113948.

Zhao, S., Danley, M., Ward, J.E., Li, D., Mincer, T.J., 2017. An approach for extraction, characterization and quantitation of microplastic in natural marine snow using raman microscopy. Anal. Methods 9, 1470–1478.

Zobkov, M., Esiukova, E., Grave, A., Khatmullina, L., 2017. Reevaluation of microplastics extraction efficiency with the aim of Munich Plastic Sediment Separator. EGU General Assembly Conference Abstracts, p. 5523.